PAPER

Check for updates

A low-cost visible and near-infrared (Vis-NIR) portable multispectral imager for fast drug analysis

Erwin Winkler Martinez, [ID] [a] Ali Tfayli,[a] Thomas Nappez,[b] Jean-Philippe Michel, [ID] [c] Douglas N. Rutledge, [ID] [a] Pierre Chaminade[a] and Sana Tfaili*[a]

The prevalence of substandard and falsified (SF) drugs requires the development of effective identification and differentiation methods to distinguish genuine from SF medications. SF drugs may have harmful consequences, including increased morbidity and mortality. Near-infrared (NIR) spectroscopy is a well-established technique that has demonstrated its effectiveness in detecting poor-quality medicines. It provides a rapid, specific, and non-destructive method for identifying SF. NIR spectroscopy may be applied in hyperspectral imaging, multispectral imaging, or point spectrum recording. Spectral NIR data, advanced data treatment, and chemometrics have proven to be essential in drug analysis. This project aimed to develop a low-cost visible and near-infrared (Vis-NIR) handheld and portable multispectral imager for fast drug analysis and detection of SF drugs. Low-cost spectrophotometers of this sort in low-income countries offer a cost-effective and quicker alternative to traditional laboratory methods (*e.g.*, mass spectrometry). For this, we analyzed paracetamol tablets (test samples) and commercial tablets. The developed device employs multispectral imaging (MSI). We processed data using Principal Components Analysis (PCA) and Independent Components Analysis (ICA). The preliminary results suggest that our prototype has promising potential, with the ability to differentiate effectively between tablets with different compositions.

1. Introduction

Multispectral imaging (MSI) has broad applications across various fields, including food analysis,[1,2] environmental monitoring, agriculture, art restoration, medical diagnostics,[3] and pharmaceutical analysis.[3–5] Capturing information across multiple wavelengths gives sufficient data to understand a sample's chemical composition and structural attributes. Ma *et al.* summarized multispectral imaging applications in ophthalmology and underlined the importance of MSI as a noninvasive technique for diagnosing retinal and choroidal disorders.[6] Bandara *et al.* developed a MSI device for food quality control applications and highlighted chemometrics' importance in detecting adulterants in turmeric powder.[7] MSI has several applications in the pharmaceutical industry: it enabled the examination of active pharmaceutical ingredient (API) distribution, excipient homogeneity, drug composition, and authenticity; and it was also used for comprehensive quality control and showed that it was possible to relate spectral data from images to physico-chemical properties.[5,8–10]

The MSI approach allows real-time and non-destructive analysis. It provides spatial and spectral information on sample composition, making it suitable for laboratory and on-site applications.[5,11] Studies show that MSI is a cost-effective and faster alternative to traditional hyperspectral imaging. Hyperspectral imaging can be used in the pharmaceutical industry to determine the homogeneity of samples.[12] Compared to MSI, it provides more information since it covers the entire spectrum, though at the cost of longer data processing times. MSI covers a few wavelengths and requires less time and computing power without compromising the relevance and quality of the data.[2] MSI research in the pharmaceutical field remains limited to studies addressing drug quality assessment.[1,3,6] The few published studies exploring multispectral imaging were in the ultraviolet (UV) range rather than NIR wavelengths.[5,8]

As it reveals physico-chemical properties, NIR imaging for drug analysis[11,13] is a promising method for ensuring therapeutic efficacy and patient safety. Vibrational spectroscopy techniques, such as NIR and Raman, are well known for the analysis of medicinal herbs and pharmaceuticals.[14–21] However, few studies have illustrated imaging applications.[11]

NIR spectroscopy, spanning wavelengths from 780 to 2500 nm, captures molecular vibrations that offer insights into drug samples' chemical and physical properties.[15,22] By comparing NIR spectra from genuine drugs with those of suspi-

*a*Université Paris-Saclay, Stratégies d'investigations analytiques: Médicaments, bioMatériaux, tissus et Matrices biologiques, 91400 Orsay, France
*b*Connected Physics, Fabrication d'équipements médicaux, 92220 Bagneux, France
*c*Université Paris-Saclay, CNRS, Institut Galien Paris-Saclay, 91400 Orsay, France

cious samples, chemometric analysis can predict concentration discrepancies and variations in excipients, aiding in the detection of substandard and falsified (SF) drugs.[23–26] Infrared spectroscopy – when combined with multispectral imaging – enables more detailed analysis of APIs and excipients, providing robust solutions for drug quality assessment and falsified drug detection.

Substandard and falsified drugs frequently appear in the global market, especially in low- and middle-income countries. The World Health Organization estimates that SF drugs constitute more than 10% of the world market, underscoring the need for practical analytical solutions.[23,27] Falsified medicines are intentionally misrepresented in composition, identity, or origin, while substandard medicines are legitimate products that fail to meet quality standards due to production errors or negligence.[27,28] Both pose serious risks to public health, contribute to drug resistance, and increase morbidity and mortality.[16] Bakker *et al.* showed all the possible analytical methods that can be applied to identify SF drugs, showing their advantages and limitations.[29] Accessible, field-deployable technology is vital, particularly for resource-limited areas. Lab-based methods (heavy benchtop devices), such as high-performance liquid chromatography (HPLC) and mass spectrometry, provide high sensitivity and selectivity, but are often not affordable and remain complex to implement in some countries.[2,26,29–31]

The literature describes the contribution of NIR and Raman vibrational methods in the fight against SF drugs.[26] The main advantage of these methods is their speed. In their study in 2005, Rodionova *et al.*, pioneering users of NIR for SF drug analysis, called it an "express method".[32] The instrumental development of handheld and portable devices accompanied the use of vibrational spectroscopy for this purpose.[21,23,27,31,33–35] Field studies generally use handheld or portable instruments to acquire point spectra. To our knowledge, no field-study addresses the use of imagers for SF drug identification.

Portable or handheld devices are designed to be simple to operate. NIR portable or handheld devices allow on-site drug analysis and provide quick spectral information that can be easily interpreted to verify authenticity. On-site analysis allows the possibility of bringing the devices to the sample. On-site analysis helps reduce time and make fast decisions for production lines and on-site investigations.[29,36] Zambrzycki *et al.* evaluated six handheld or portable devices for point spectra (NIR or Raman), discussing the limitations and advantages of each.[37] They presented an interesting perspective on the cost of devices, as well as all the extra charges that also add up (such as consumables, computers, *etc.*). None of these devices is currently in use for on-field identification of SF drugs due to their high cost or low performance. In the literature, all current devices being evaluated are for point spectra, with only one imager device, the CDx,[38] being identified, which remained at the proof-of-concept stage and was never commercialized.[39]

In the present work, we aim to develop a low-cost, portable visible and near-infrared (Vis-NIR) multispectral imager for fast drug analysis and identification of SF drugs. The use of low-cost portable spectrophotometers in low- and middle-income countries offers a cost-effective and quicker method than alternative standard laboratory methods. The first tests were conducted on two commercial samples – Doliprane® and Pentasa® –, coated tablets, and paracetamol tablets. Paracetamol samples were produced in the laboratory to ensure precise percentages of API and excipients, following European Pharmacopeia guidelines for pharmaceutical characterization. Two different formulations, 0% API and 100% API, respectively, were prepared to emulate SF products. Six samples were taken for each formulation – A16 to A21 for 0% and E23 to E27 for 100% – to ensure repeatability. The device was also tested to analyze commercial tablets, including Doliprane D01, Pentasa P01, and coated tablets R01. We defined a range of spectral bands using 13 LEDs spanning from 450 nm to 1085 nm to build the first version of our prototype. For data treatment, we used chemometric tools and multivariate analysis. The potential of our portable MSI prototype, as an effective solution for low-cost and rapid drug analysis, was demonstrated.

2. Methodology

2.1. Samples

Two commercially available samples were selected Doliprane® and Pentasa® (SI S1), and red-coated tablets (SI S1) without API. Paracetamol tablets were prepared with API (100%) and without API (0%). All tablets were characterized following the European Pharmacopeia guidelines.[40] Table 1 shows the proportions of API and excipients to prepare 250 grams of powder by wet granulation. The 0% formulation comprises 100 grams of Avicel PH 102 instead of API and is prepared by direct compression.

2.2. Multispectral imaging system ("prototype")

The first version of a multispectral imaging system was built based on wavelengths selected from the visible to NIR region of the electromagnetic spectrum. As shown in Fig. 1A, the system comprises a 1-megapixel (1280 × 800) monochromatic camera (OmniVision, Santa Clara, California, USA). The camera sensor features an image array capable of operating at up to 120 frames per second (fps) in 10-bit color. The sensors' technology removes common sources of image contamination - inlcuding noise and smearing - resulting in a clean, stable image. In the center of the circuit board (green) and 13 LEDs (Thorlabs Newton, New Jersey, USA) distributed around it (with peaks at wavelengths 450, 525, 610, 750, 810, 850, 870, 890, 930, 940, 970, 1050, and 1085 nm). The LEDs are evenly distributed to provide homogeneous illumination around the sample (4 LEDs per wavelength). A hinged arm holds the prototype (Fig. 1B) to control the height and rotation of the device. The incorporation of more LEDs in the NIR range enables the acquisition of additional spectral information.

Table 1 Distribution of API and excipients by mass for each formulation of paracetamol tablets. For the 0% (A) formulation the API is replaced by Avicel PH 102(VIVAPUR®) and for the 100% (E) formulation the API is paracetamol

Category Supplier Chemicals	API RHODAPAP® Paracetamol (grams)	Excipient JRS PHARMA® Emcompress (grams)	Excipient Cooper® Wheat starch (grams)	Lubricant Cooper® Magnesium stearate (%)	Disintegrant SPCI® Explotab (%)
Test tablet 100% API (E) Samples E22–E27	100	100	50	1	2
Test tablet 0% API (A) Samples A16–A21	0	100	50	1	2
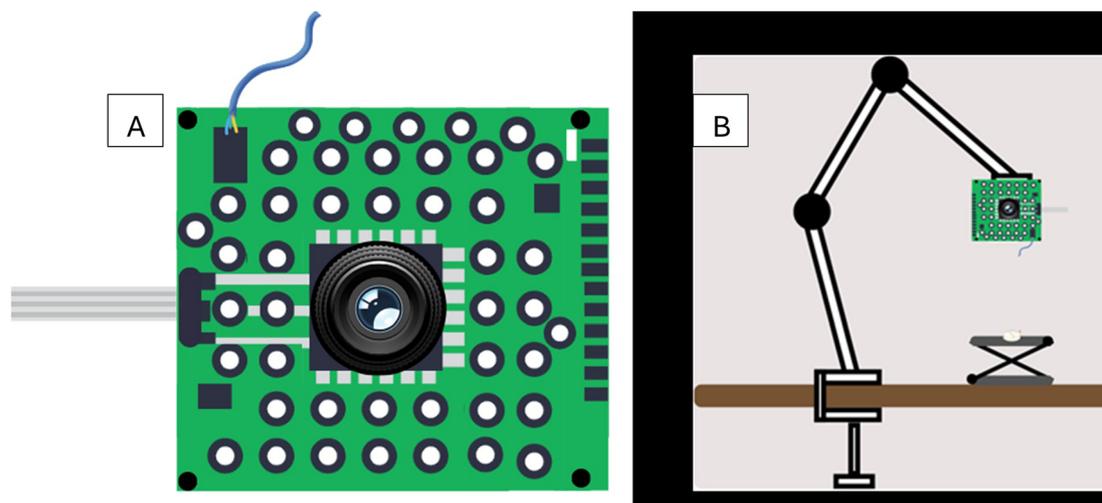
Fig. 1 (A) Sketch of the prototype and distribution of the LEDs. (B) Diagram showing the prototype and the arm stand; the orientation of the prototype facing the front is just for easier understanding. The prototype LEDs and camera were placed facing downwards, pointing to the location of the sample.

Samples were placed on a plate below, and images were recorded using each LED alone once the camera parameters were set. The exposure time was set *via* shutter control (acquisition time), and the sensor signal from each pixel is processed to correct the offset and multiply the data by the corresponding gain (intensity of brightness). Each LED has its own combination of acquisition time and gain (see the SI section and Table S1); acquiring each image took between 10 and 15 seconds (an image per LED is acquired). All experiments were conducted inside a lightproof enclosure. Multiple tablets of varying physicochemical properties were also tested (Section S1, SI data). We also recorded images with all LEDs in the visible range turned on, with LEDs in the NIR range turned on, and with all the LEDs on for visual inspection.

2.3. Data processing

Data processing, computations, and chemometric analyses were performed using in-house scripts written in Matlab R2014b (The MathWorks, Inc., Natick, MA, USA).

2.3.1. Pre-processing. We used a Matlab script to crop all tablet images to the exact dimensions, removing the background and isolating only the tablets. After this uniform cropping, we proceeded to analyze a single tablet (Fig. 2) using Principal Components Analysis (PCA) to identify regions containing outlier pixels (Section 2.3.2).

2.3.2. Principal components analysis (PCA). PCA is an unsupervised method that allows the exploration and reduction of the dimensionality of a multivariate dataset. Linear combinations of the initial variables are computed, called Principal Components (PCs). PCA constructs PCs to extract the maximal variance in the dataset, with the first PC representing the direction of the greatest dispersion of the samples in the multidimensional space defined by the variables. The process is sequential, with each subsequent PC oriented orthogonally to the previous ones to extract the maximum of the remaining variance. PCA helps simplify and highlight the key patterns and relationships within complex datasets. It reveals groups, outliers, drift within the data, and similarities among samples and variables.[25,41]

A few spectra originating from the 0% API tablet formed a separate cluster in the PCA plot (the region between 0 and 200 in PC1). This cluster corresponded to spectra located at the tablet borders. By isolating these outlier pixels, we generated an image and a corresponding mean spectrum. This analysis confirmed that the outlier pixels were associated with the tablet edges (Fig. 2). These pixels were subsequently identified and removed from all images before starting the processing. PCA was used for both pre-processing and processing.
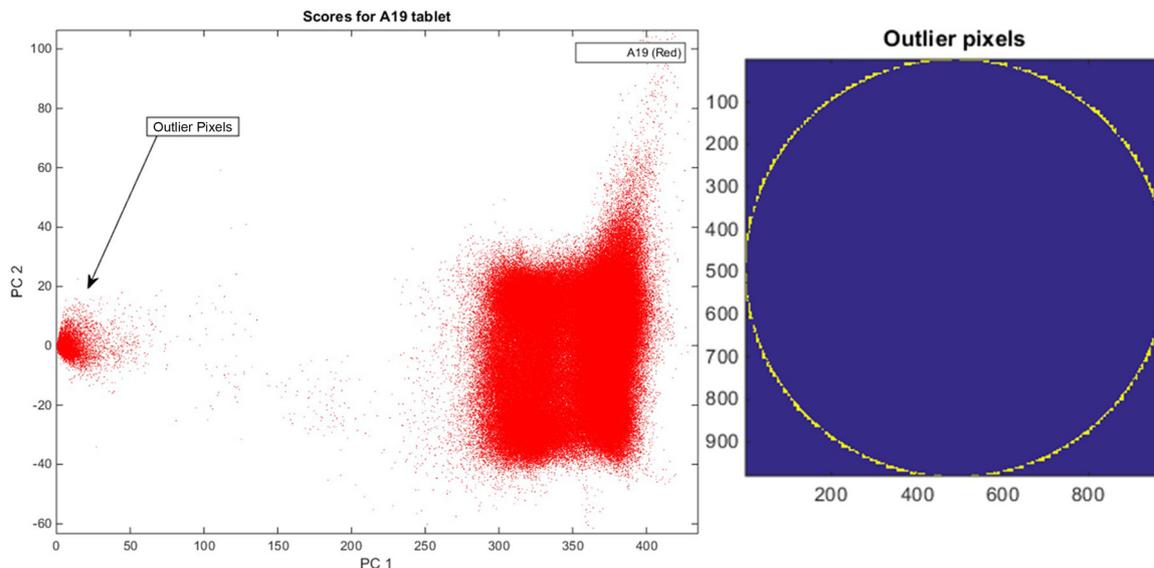
Fig. 2 Score plot of PC1 *vs.* PC2 for a tablet at 0% API, used to identify the location of outlier pixels—the corresponding pixels are highlighted in yellow, and are located at tablet borders.

2.3.3. Independent components analysis (ICA). ICA is an unsupervised technique that enables the exploration of high-dimensional multivariate datasets. It reduces the dimensionality of the data by calculating Independent Components (ICs), which are also linear combinations of the original variables, while maximizing the statistical independence of these components. The process involves identifying components that exhibit non-Gaussian distributions and are mutually independent, providing a more interpretable representation of the data compared to that with methods that focus solely on variance (as does PCA). ICA aids in uncovering hidden factors and intricate structures embedded within datasets.[42] This approach helps to avoid reliance on classification methods that require reference spectra.

2.4. Additional statistical tests

To confirm the contribution of each LED showing to be significant after running PCA and ICA, and to confirm the contribution of LEDs in the NIR range, we extracted the loadings of the principal component showing the separation in PCA results, and of the independent component showing the separation in ICA results. The loadings of these PC and IC were extracted considering the whole set of LEDs.

Statistical analyses including histograms for data distribution visualization, *t*-tests for group comparisons (each group included 0% and 100% API test tablets), and Cohen's *d* to measure the distance in each group were performed.

We also ran PCA and ICA on reconstructed images for LEDs in the visible range alone, and then on reconstructed images for LEDs in the NIR range alone. Similarly, we extracted the loadings of the principal component showing the separation in PCA results, and of the independent component showing the separation in ICA results. This time, the loadings of these PC and IC covered the LEDs in visible or in NIR ranges. We

applied also statistical analyses including histograms for data distribution visualization, *t*-tests for group comparisons (each group included 0% and 100% API test tablets), and Cohen's *d* to measure the distance in each group.

3. Results and discussion

Images were acquired on 15 tablets. The tablets were chosen based on their different physicochemical properties. The differences in shape, size, and color helped us understand the limits of the prototype and the parameters to consider when recording images. For the remainder, we analyzed test tablets prepared in the laboratory containing excipients and 100% or 0% API, and commercially available tablets Doliprane® and Pentasa® as well as red-coated tablets without any API inside. Fig. 3 shows the images for each LED individually and the combination of the visible range LEDs, NIR range LEDs, and all LEDs together for visual inspection. For each image, the shutter and gain must be set to balance the exposure (SI Table S1). The image quality decreased with the last two LEDs due to their proximity to the sensor's limits. Images of the commercial samples (Doliprane®, Pentasa® and red-coated tablets) are provided in the SI Section Fig. S1–S3.

Data processing was done on six tablets with 0% API (labelled A and numbered A16–A21) and six tablets with 100% (labelled with the letter E and numbered E22–E27), using only the images with the LEDs from 450 to 970 nm.

Since the image captured by the device is larger than the tablet and thus contains useless information, we cropped the images to the tablet's dimensions. Cropping the images allows us to focus on the region where the sample is located and extract relevant intensity data. All the images were cropped to the same dimensions. This pre-processing was followed by PCA to remove outliers. As shown in Fig. 3, each image provides
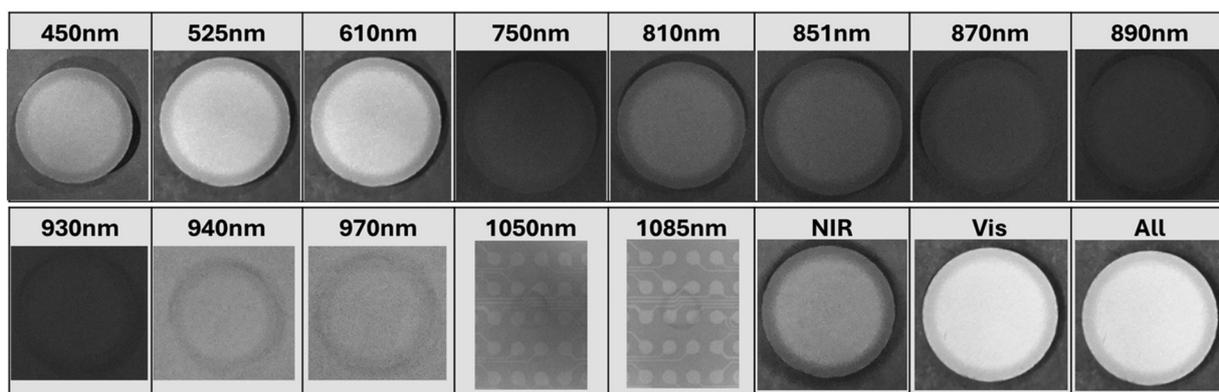
Fig. 3 Images of a 0% paracetamol tablet acquired with the prototype: individual LED illumination, followed by LEDs in the visible range, NIR range, and all LEDs combined. Although the system includes 13 LEDs, only 11 are used for image processing. The 1050 nm and 1085 nm LEDs were excluded because their images show reflections and distortions likely due to their proximity to the sensor's spectral limits, which obscure the tablets, as shown in the figure. The visible, NIR, and all LED images are shown for visual inspection to assess whether these artifacts occur only when these LEDs operate individually or also when combined with others.

spectral and spatial information, capturing variations in intensity across wavelengths and space. The multispectral image of each tablet was generated by overlaying the images recorded from each LED alone. This created a data cube. Images from each data cube were concatenated before PCA and ICA processing. PCA and ICA were conducted on data cubes in pairs.

3.1. Principal components analysis

PCA was applied to multispectral images to identify patterns and reduce dimensionality. To ensure repeatability, we used 12 tablets (refer to Table 1): six tablets with 100% API (E22–E27) and six tablets with 0% API (A19–A22), comparing them in pairs to create multiple repetitions. This allowed us to evaluate the con-

sistency between the two tablets groups. Doliprane® (labelled D01), Pentasa® (labelled P01) and red-coated tablets (labelled R01) were compared with test tablets at 100% API (E25).

The optimal number of principal components (PCs) was found to be 5, using the random PCA method.[31] Fig. 4 presents the scatter plot for the first and second component (samples A19 and E25), showing a clear separation between 100% (Yellow) and 0% (Blue) tablets. PC2 separates almost completely the two groups while PC1 also gives a partial separation; this is corroborated with the 1D score plot of component 2 (Fig. 4). As illustrated in the plot images in the supplementary data (Fig. S12) and the score plots (Fig. S14). This indicates that these two PCs contain information that helps us distinguish between both
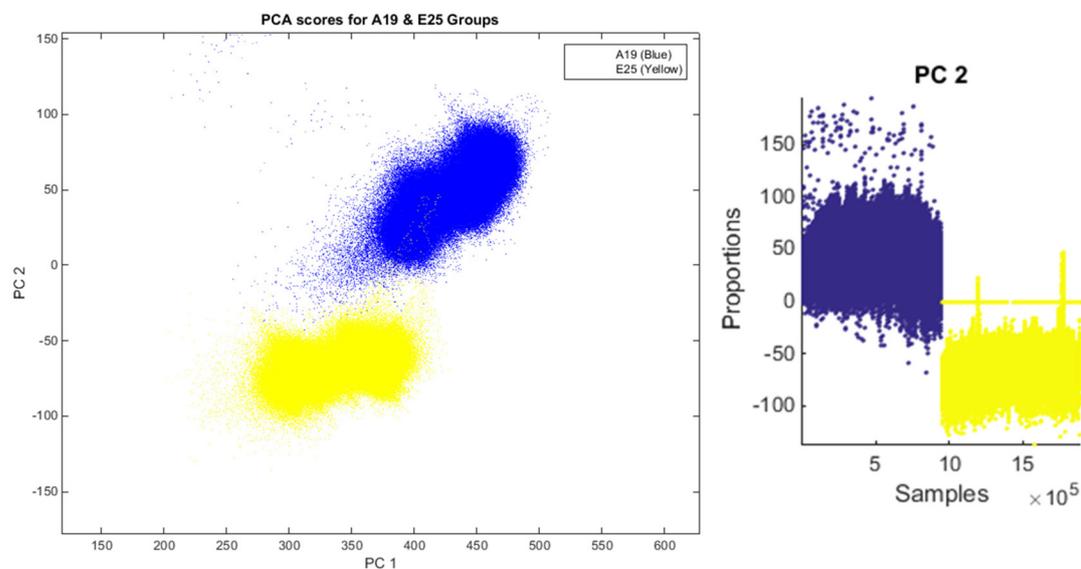

Fig. 4 2D scatter plot illustrated for PC1 and PC2 for 0% (A19) and 100% (E25) API test tablets: blue represents 0% and yellow represents 100%. The 1D score plot of PC2 across the pixel position for A19 (blue) and E25 (yellow) tablets illustrates that PC2 is responsible for the separation between tablets.
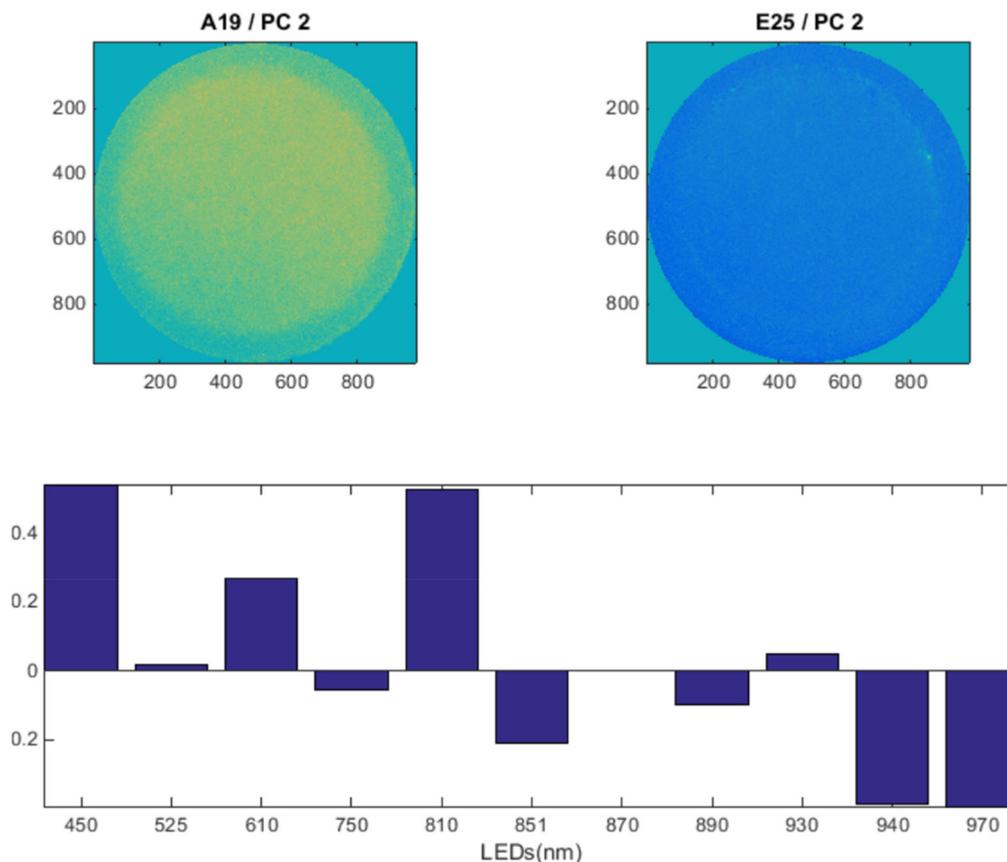
Fig. 5 Plots of PCA images and plot of the multispectral response for 0% (A19) and 100% (E25) API test tablets. Each image represents the contribution of PC2. The blue bars illustrate each LED contribution from 450 to 970 nm.

samples. Fig. 5 presents the PC2 image plots, visualizing the intensity difference between the two samples. The bar plot in Fig. 5 shows the contribution of each LED in the selected range. The highest contributions are obtained with positive values from 450 nm (blue light), 610 nm (red light) and 810 nm (NIR) light, indicating a higher signal from the 0% tablets for these three wavelengths, followed by negative values for 851 nm, 940 nm and 970 nm (NIR) light, indicating a higher contribution from the 100% API tablet (SI Fig. S12 shows PC1–PC5). Fig. 6 and 7 show the comparison between a Doliprane® tablet and a 100% API tablet. The scatter plot (Fig. 6) presents the first and second components, showing a clear separation between 100% API test (green) and Doliprane® (red) tablets. For Doliprane® compared to the 100% API test sample, the results showed the highest positive contributions at values 450 nm (blue light), 810 nm (NIR) and 870 nm (NIR), indicating a higher signal from the Doliprane® tablet for these three wavelengths, followed by negative values for 851 nm, 940 nm and 970 nm (NIR), indicating a higher contribution from the 100% API tablet (Fig. 7).

3.2. Independent components analysis

For ICA, we followed the same process as for PCA to analyze the data and extract the independent components (ICs). 5 ICs were selected based on their reproducibility across multiple ICA runs
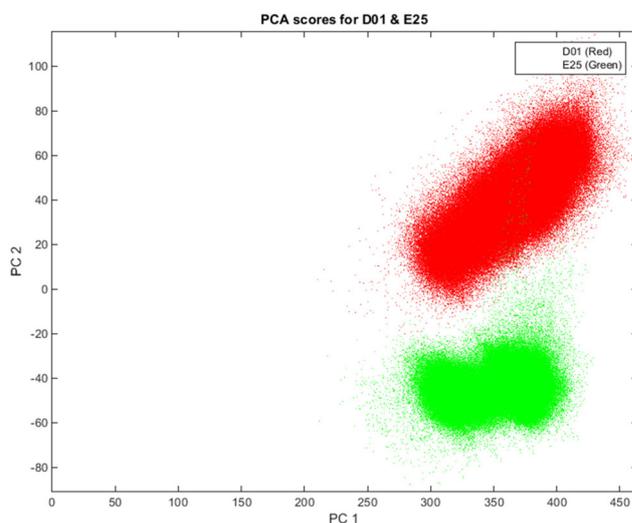

Fig. 6 Scatter plot illustrated for PC1 and PC2 for Doliprane® (D01) and 100% API test tablets (E25). Each color represents a tablet: red (Doliprane®) and green (100% API test tablet).

using the random ICA method.[43] Component 3 exhibited the greatest separation among the 5 calculated components. Components 2, 4, and 5 also displayed some separation; see SI
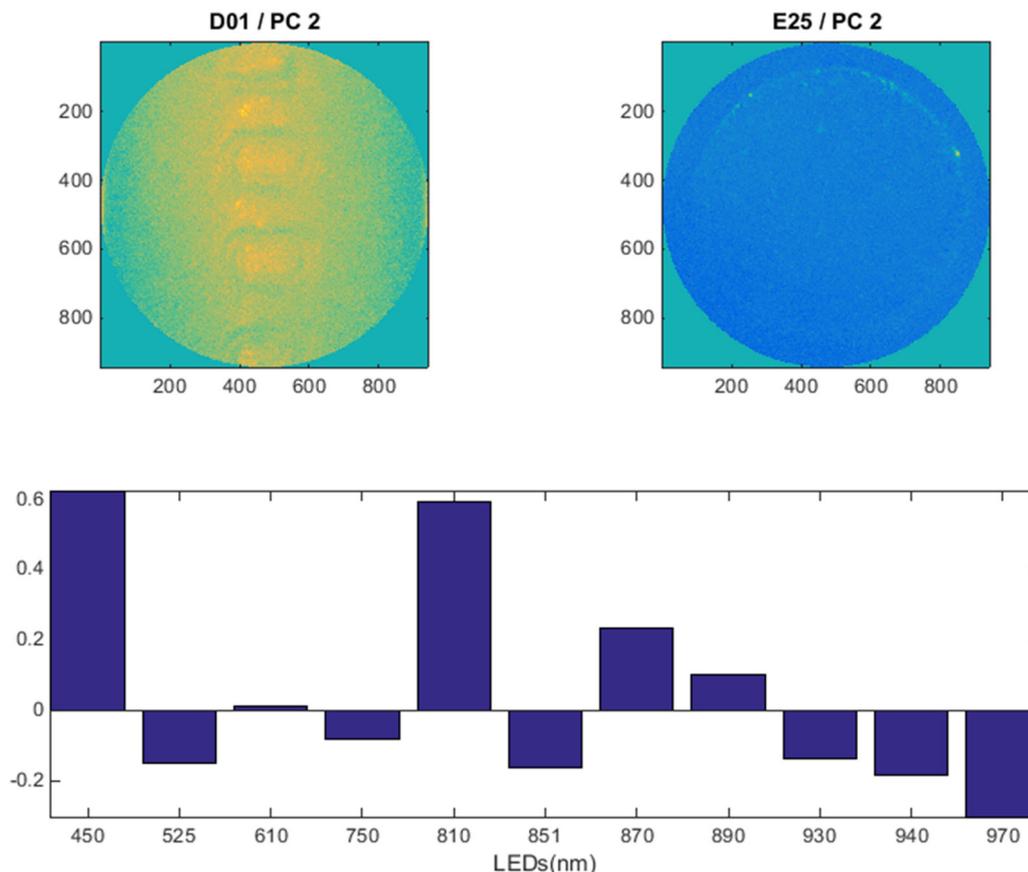
Fig. 7 Plots of PCA images and plot of the multispectral response for Doliprane® (D01) and for 100% API test tablets (E25). Each image represents the contribution of PC2. Doliprane® reconstructed image on PC2 illustrates clearly the imprint on the tablet. The blue bars in the last part of the figure illustrate each LED contribution from 450 to 970 nm.

S17. Fig. 8 shows the scatter plot for IC2 and IC3, illustrating the clear separation between the 100% (yellow) and 0% (blue) tablets (samples A19 and E25). IC3 separated completely the two groups while IC2 did not. This suggests that the information related to the API is prominently captured by IC3. This is corroborated with the 1D score plot of component 3 (Fig. 8). As displayed in the plot images (SI Fig. S13) and the score plots (SI Fig. S15), the primary separation is attributed to IC3, although 2, 4 and 5 also exhibit minor separation and variation in color intensity. Fig. 9 shows the plot of IC3 for each tablet. This component enabled us to distinguish between the two concentrations based on differences in their intensities. The bar plot in Fig. 9 shows the contribution of each LED in the selected range. The highest positive contributions in IC3 are obtained from 450 nm and 810 nm light, respectively, as shown in PCA results (Section 3.1). In contrast to PCA results, 610 nm, 940 nm and 970 nm light had weak contributions. The NIR signal at 851 nm presents a negative contribution to IC3, indicating a higher contribution from the 100% API test tablet.

Fig. 10 and 11 show the comparison between a Doliprane® tablet and a 100% API test tablet. The scatter plot (Fig. 10) presents the sixth and seventh components, showing a clear separation between 100% API test tablets (green) and Doliprane®

(red) tablets. The highest positive contributions at values 450 nm (blue light), 810 nm (NIR), 870 nm (NIR) and 890 nm (NIR) indicate a higher signal from the Doliprane® tablet for these four wavelengths (Fig. 7).

The presented home-built prototype – which uses LEDs and a monochromatic camera to capture multispectral images – demonstrated its potential (to differentiate samples) through a multivariate analysis. Both methods, PCA and ICA, helped to differentiate between 0% API (A16–A21) and 100% API (E22–E27) formulations. Moreover, the comparison between Doliprane® (D01), Pentasa® (P01), in SI Fig. S4, S5, S8 and S9, and red-coated tablet (R01), in SI Fig. S6, S7, S10 and S11, with our 100% API test tablet (E25) formulation showed promising results. While both PCA and ICA have their mathematical foundation, both provided relevant information. First, to discriminate between the samples and second, to understand which LEDs provided the most relevant information. Given the similar outcomes, using a single chemometric approach may be sufficient in future applications, especially when it comes to fast drug analysis. It is worth mentioning that when using ICA, a higher number of LEDs and stronger intensity signals were involved in discrimination. Comparing the signals from both methods could guide future optimization of LED selection and system configuration.
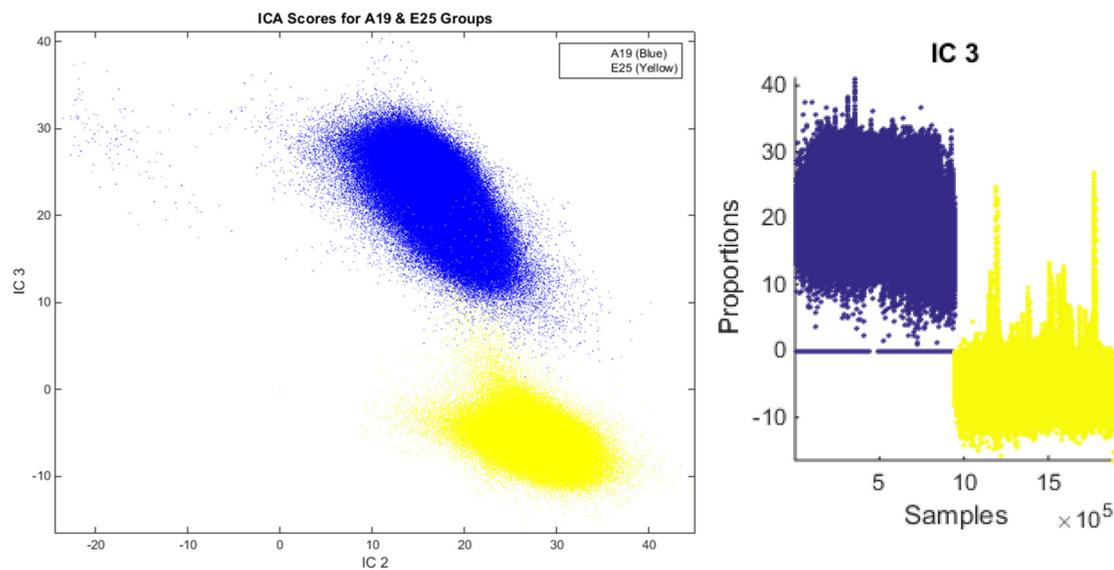
Fig. 8 2D scatter plot illustrated (left) for IC2 and IC3 for 0% (A19) and 100% API test tablets (E25): blue represents 0% and yellow represents 100%, with no strange pixels. The 1D score plot (right) of IC3 across the pixel position for A19 (blue) and E25 (yellow) illustrates that IC3 is responsible for the separation between tablets.
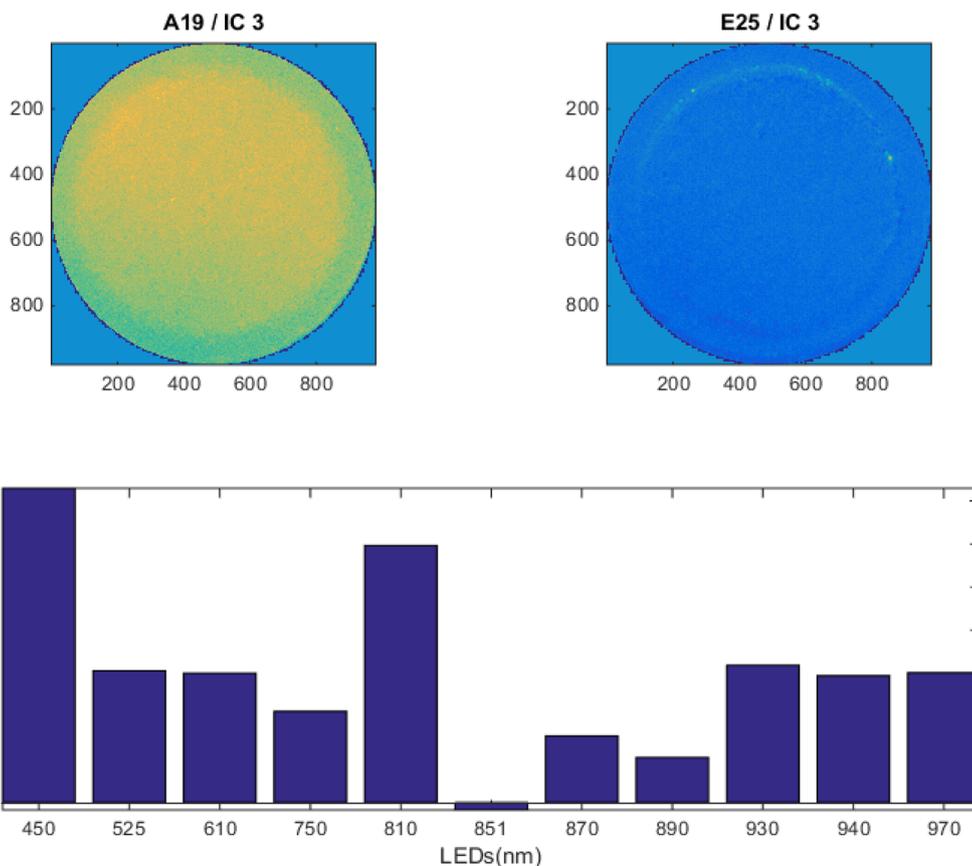

Fig. 9 Plots of ICA images and plot of the multispectral response for 0% (A19) and 100% (E25) API test tablets. Each image represents the contribution of IC2. The blue bars illustrate each LED contribution from 450 to 970 nm.
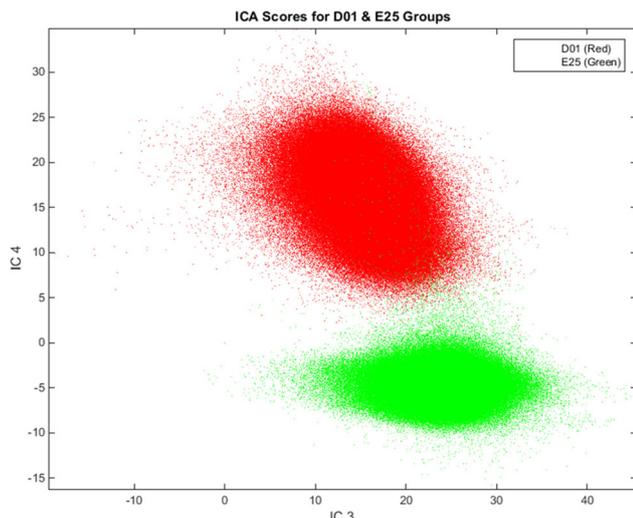
Fig. 10 Scatter plot illustrated for IC4 and IC3 for Doliprane® (D01) and 100% API test tablet (E25). Each color represents a tablet: red (Doliprane®) and green (100% API test tablet).

Overall, integrating a multivariate analysis, employing only a few wavelengths, a low-cost, image-based MSI camera offers a practical fast solution for drug control. Notably, while many commercial systems are limited to point spectra or designed for different types of samples, our setup enables direct image capture (MSI). With minimal spectral input and straightforward chemometric techniques, we could differentiate between tablets with close but different formulations.

3.3. Comparison of discriminative power: additional statistical tests

To assess the capabilities of our device and demonstrate that it captures meaningful spectral information beyond the visible range, we performed PCA and ICA separately on data recorded in the visible and NIR regions. We extracted the loadings of two tablets (samples A19 and E25); the principal component showed the separation in PCA results, and the independent component showed the separation in ICA results (samples A19 and E25). We also extracted the loadings of PC and IC considering the whole set of LEDs.

Fig. 12A and B illustrate the histograms and Cohen's *d*-test values using the full dataset covering all LEDs. The pixel intensities for PC2 or for IC3 loadings are shown in these figures.
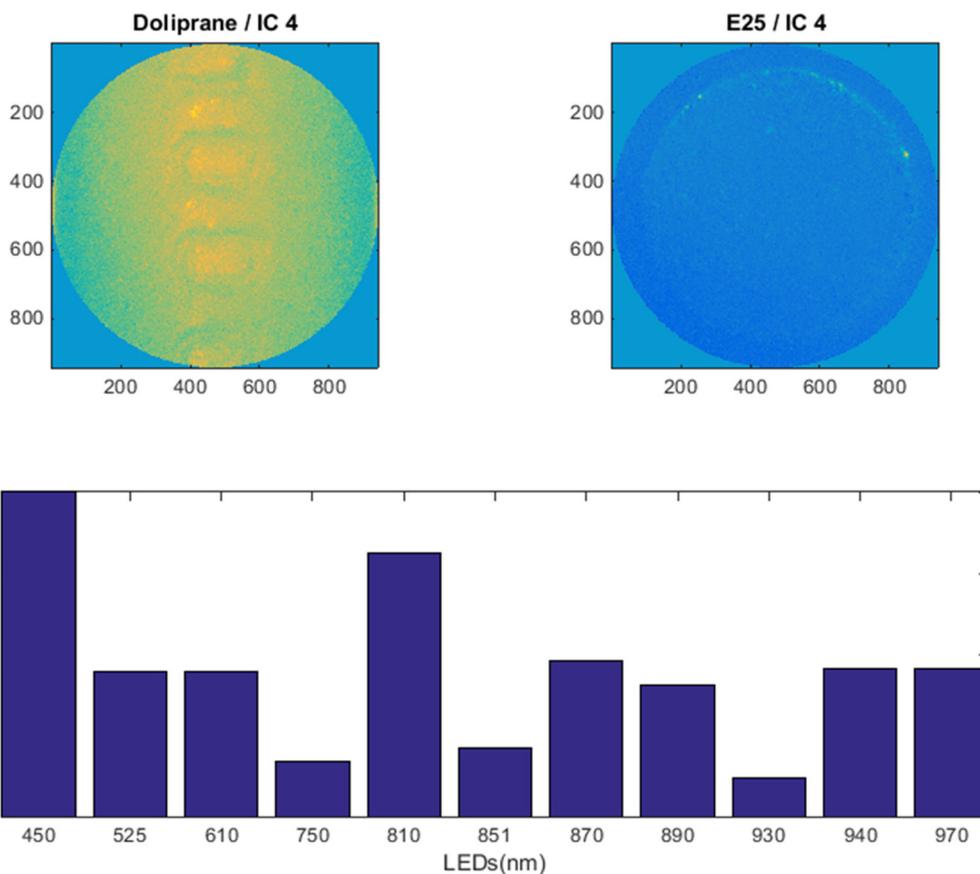

Fig. 11 Plots of ICA images and plot of the multispectral response for Doliprane® (D01) and 100% API test tablet (E25). Each image represents the contribution of IC4. Doliprane® reconstructed image on IC4 illustrates clearly the imprint on the tablet. The blue bars illustrate each LED contribution from 450 to 970 nm.
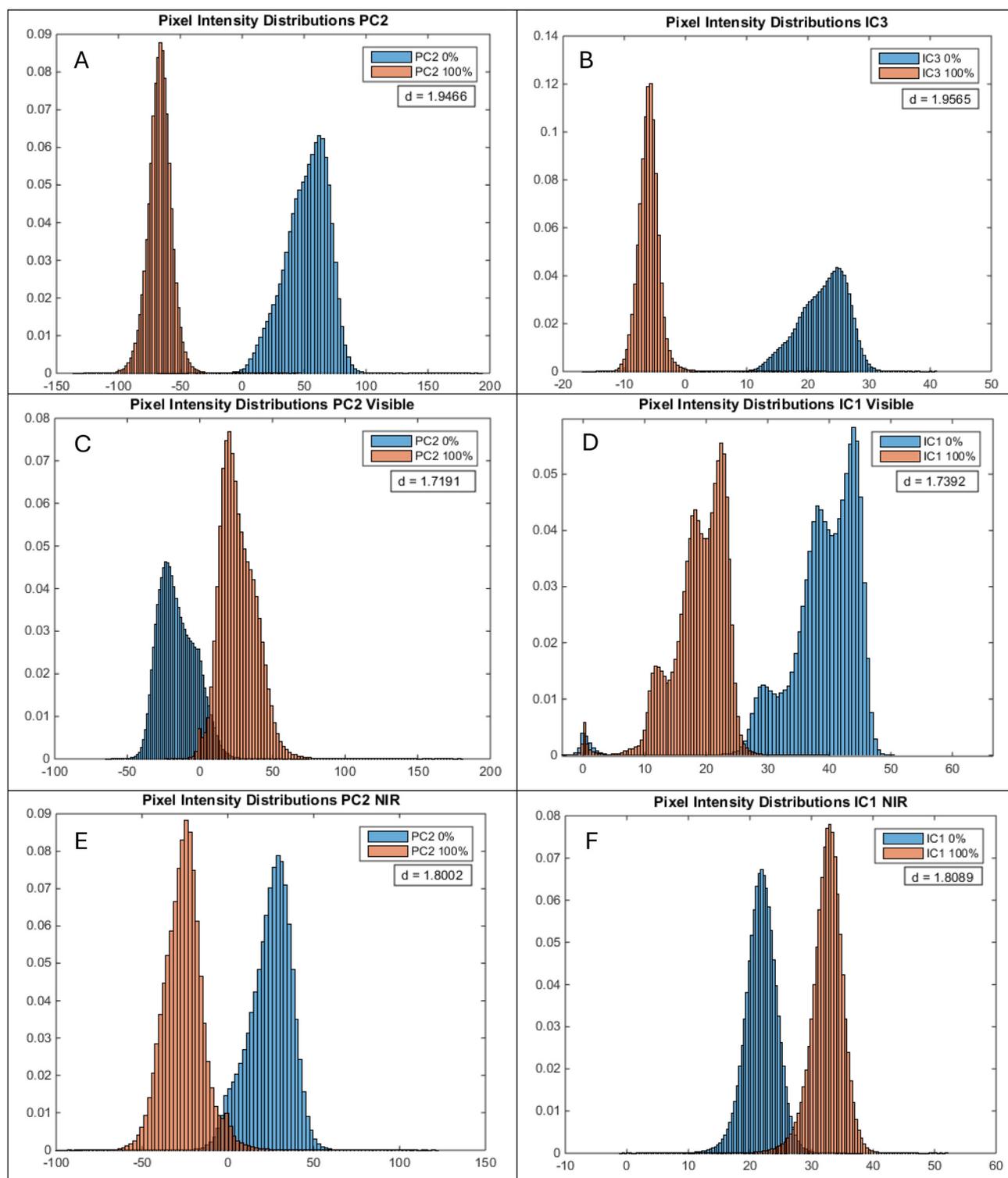
Fig. 12 Histogram results and corresponding Cohen's *d*-values comparing pixel intensities for multispectral data of two test tablets (samples A19 and E25), with 0% API (blue) and 100% API (orange). Histograms of pixel intensities for PC2 using all LEDs (A), considering the visible range (C) and the NIR range (E). Histogram of pixel intensities for IC3 using all LEDs (B), and histograms of pixel intensities for IC1 considering the visible range (D), and the NIR range (F). Higher Cohen's *d* values indicate stronger discriminative power.

The analysis of the outputs – for the second principal component (PC2) and third independent component (IC3) – highlighted the separation between samples, with d-values equal to 1.9466 (pixel intensities for PC2 loading) and 1.9565 (pixel intensities for IC3 loading).

Fig. 12C and D illustrate the histograms and Cohen's d-test values using the visible range (450, 525, 610, and 750 nm LEDs). When running PCA and ICA on data in the visible range, PC2 and IC1 loadings appeared to be the components separating between the groups. As illustrated, pixel intensities for PC2 or for IC1 loadings are separated between samples, with d-values equal to 1.7191 (pixel intensities for PC2 loading) and 1.7392 (pixel intensities for IC1 loading).

Fig. 12E and F illustrate the histograms and Cohen's d-test values using the NIR range (810, 851, 870, 890, 930, 940 and 970 nm LEDs). When running PCA and ICA on data in the NIR range, PC2 and IC1 loadings were found to be the components separating between the groups. As illustrated, pixel intensities for PC2 or for IC1 loadings are separated between samples, with d-values equal to 1.8002 (pixel intensities for PC2 loading) and 1.8089 (pixel intensities for IC1 loading).

The distance measurement with Cohen's d-test revealed significant separation between the two groups in all pixel's intensities for PCA and ICA, having the highest value in the whole data set and the lowest value of separation in the visible range.

The t-test (p-value) showed a significant difference for the whole data set (pixel intensities for PC2 and IC3 loadings), visible range (pixel intensities for PC2 and IC1 loadings), and NIR range (pixel intensities for PC2 and IC1 loadings).

The results support the idea that recording multispectral data provides more discriminative information than working only in the visible range. It is important to note that our device's camera is not a standard RGB camera. Our camera covers a wider range of the spectrum, allowing us to extract spectral information beyond the visible range. We need to continue working on our portable prototype: optimizing, improving and acquiring images with multiple samples.

4. Conclusion

In this feasibility study, we demonstrated the capability of our multispectral prototype to capture images and discriminate between groups of tablets. The results are promising for both test samples (tablets produced in the laboratory with 0% API or 100% API, and excipients), as well as tablets from the market (Doliprane®, Pentasa®, and a red-coated tablet) with various physicochemical properties. These initial results suggest that the present fast, portable, and future handheld imaging prototype has promising potential, with the ability to differentiate effectively between tablets with different compositions. The results confirmed the interest in using LEDs from both visible and NIR ranges. In perspective, we will continue to optimize the device – with different LEDs and other chemometric tools – and test it in a broader range of samples.

These initial findings highlight the novelty of the device and its potential for further development in identifying SF drugs. The optimization and development of this low-cost device could provide valuable support in detecting substandard and falsified drugs in low- and middle-income countries.

Conflicts of interest

There are no conflicts to declare.

Data availability

The data supporting the findings of this study are available within the article and the supplementary information (SI). Supplementary information is available. See DOI: https://doi.org/10.1039/d6an00059b.

Additional data are available from the corresponding author upon request.

Acknowledgements

References

1 M. Kharbach, M. Alaoui Mansouri, M. Taabouz and H. Yu, *Foods*, 2023, **12**, 2753.
2 W. G. C. Chaminda Bandara, G. Prabhath, D. M. K. V. B. Dissanayake, H. Herath, G. Godaliyadda, M. Ekanayake, S. Demini and T. Madhujith, *J. Food Eng.*, 2020, **266**, 109700.
3 Z. Lin, X. Hu, Y. Liu, S. Lai, L. Hao, Y. Peng, Y. Li, Z. Zhu, X. Huang, K. Huang and M. Zhang, *Heliyon*, 2024, **10**, e36389.
4 M. Vidal and J. M. Amigo, *Chemom. Intell. Lab. Syst.*, 2012, **117**, 138–148.
5 A. Novikova, J. M. Carstensen, T. Rades and C. S. Leopold, *Int. J. Pharm.*, 2016, **515**, 374–383.
6 F. Ma, M. Yuan and I. Kozak, *Surv. Ophthalmol.*, 2023, **68**, 889–904.
7 W. G. C. Bandara, G. Prabhath, D. M. K. V. B. Dissanayake, V. Herath, G. Godaliyadda, M. Ekanayake, D. Demini and T. Madhujith, *J. Food Eng.*, 2020, **266**, 109700.
8 M. Klukkert, J. X. Wu, J. Rantanen, J. M. Carstensen, T. Rades and C. S. Leopold, *Eur. J. Pharm. Sci.*, 2016, **90**, 85–95.
9 S. Wilczyński, R. Koprowski, M. Marmion, P. Duda and B. Błońska-Fajfrowska, *Talanta*, 2016, **160**, 1–8.
10 I. Malik, M. Poonacha, J. Moses and R. A. Lodder, *AAPS PharmSciTech*, 2011, **2**(2), 38–44.

11 M. Boiret and F. Chauchard, *Anal. Bioanal. Chem.*, 2017, **409**, 683–691.

12 J. G. Rosas, S. Armenta, J. Cruz and M. Blanco, *Anal. Chim. Acta*, 2013, **787**, 173–180.

13 C. Caillet, S. Vickers, S. Zambrzycki, N. Luangasanatip, V. Vidhamaly, K. Boutsamay, P. Boupha, Y. Lubell, F. M. Fernández and P. N. Newton, *PLoS Neglected Trop. Dis.*, 2021, **15**, e0009287.

14 M. Jamrógiewicz, *J. Pharm. Biomed. Anal.*, 2012, **66**, 1–10.

15 H. Chen, Z. Lin and C. Tan, *Anal. Biochem.*, 2020, **590**, 113514.

16 O. Awotunde, N. Roseboom, J. Cai, K. Hayes, R. Rajane, R. Chen, A. Yusuf and M. Lieberman, *Anal. Chem.*, 2022, **94**, 12586–12594.

17 K. Dégardin, A. Guillemain, N. V. Guerreiro and Y. Roggo, *J. Pharm. Biomed. Anal.*, 2016, **128**, 89–97.

18 M. M. Kimani, A. Lanzarotta and J. S. Batson, *J. Forensic Sci.*, 2021, **66**, 2167–2179.

19 J. Kos, D. Pavelek, M. Kaykhaii, M. Olsen, J. Jampilek and R. Halko, *Eur. J. Pharm. Sci.*, 2025, **212**, 107175.

20 A. K. Rai, S. Khan, A. Kumar, B. K. Dubey, R. K. Lal, A. Tiwari, P. K. Trivedi, C. T. Elliott and R. Ch, *Metabolites*, 2023, **13**, 122.

21 H. Rais, P. Esseiva, O. Delémont, C. Schelling, S. Stanojevic, S. Rudaz and F. Coppey, *J. Pharm. Biomed. Anal.*, 2025, **263**, 116940.

22 R. Deidda, P.-Y. Sacre, M. Clavaud, L. Coïc, H. Avohou, P. Hubert and E. Ziemons, *TrAC, Trends Anal. Chem.*, 2019, **114**, 251–259.

23 P. H. Ciza, P.-Y. Sacre, M. R. Kanyonyo, C. T. Waffo, M. A. Borive, L. Coïc, J. K. Mbinze, P. Hubert, E. Ziemons and R. D. Marini, *Talanta Open*, 2021, **3**, 100025.

24 O. Y. Rodionova, L. P. Houmøller, A. L. Pomerantsev, P. Geladi, J. Burger, V. L. Dorofeyev and A. P. Arzamastsev, *Anal. Chim. Acta*, 2005, **549**, 151–158.

25 J. Luypaert, D. L. Massart and Y. Vander Heyden, *Talanta*, 2007, **72**, 865–883.

26 H. Rebiere, P. Guinot, D. Chauvey and C. Brenier, *J. Pharm. Biomed. Anal.*, 2017, **142**, 286–306.

27 C. A. Waffo Tchounga, P.-Y. Sacré, P. Ciza Hamuli, R. Ngono Mballa, C. De Bleye, E. Ziemons, P. Hubert and R. Marini Djang'eing'a, *Am. J. Trop. Med. Hyg.*, 2023, **108**, 403–411.

28 S. Assi, B. Arafat, K. Lawson-Wood and I. Robertson, *Appl. Spectrosc.*, 2021, **75**, 434–444.

29 I. M. E. Bakker-'t Hart, D. Ohana and B. J. Venhuis, *J. Pharm. Biomed. Anal.*, 2021, **197**, 113948.

30 C. Caillet, S. Vickers, V. Vidhamaly, K. Boutsamay, P. Boupha, S. Zambrzycki, N. Luangasanatip, Y. Lubell, F. M. Fernández and P. N. Newton, *PLoS Med.*, 2021, **18**, e1003747.

31 A. Guillemain, K. Dégardin and Y. Roggo, *Talanta*, 2017, **165**, 632–640.

32 O. Y. Rodionova, L. P. Houmøller, A. L. Pomerantsev, P. Geladi, J. Burger, V. L. Dorofeyev and A. P. Arzamastsev, *Anal. Chim. Acta*, 2005, **549**, 151–158.

33 B. K. Wilson, H. Kaur, E. L. Allan, A. Lozama and D. Bell, *Am. Soc. Trop. Med. Hyg.*, 2017, **96**, 1117–1123.

34 C. A. Waffo Tchounga, R. D. Marini, E. Nnanga Nga, P. Ciza Hamuli, R. Ngono Mballa, P. Hubert, E. Ziemons and P.-Y. Sacré, *Appl. Spectrosc.*, 2023, **77**, 1264–1279.

35 L. Roth, K. B. Biggs and D. K. Bempong, *AAPS Open*, 2019, **5**, 2.

36 N. Luangasanatip, P. Khonputsa, C. Caillet, S. Vickers, S. Zambrzycki, F. M. Fernández, P. N. Newton and Y. Lubell, *PLoS Neglected Trop. Dis.*, 2021, **15**, e0009539.

37 S. C. Zambrzycki, C. Caillet, S. Vickers, M. Bouza, D. V. Donndelinger, L. C. Geben, M. C. Bernier, P. N. Newton and F. M. Fernández, *PLoS Neglected Trop. Dis.*, 2021, **15**, e0009360.

38 J. S. Batson, D. K. Bempong, P. H. Lukulay, N. Ranieri, R. D. Satzger and L. Verbois, *Malar. J.*, 2016, **15**, 119.

39 CBS news FDA develops handheld device to spot fake malaria drugs, The Associated Press, 2013.

40 Édition de la Pharmacopée Européenne, *European Directorate for the Quality of Medicines & HealthCare (EDQM)*, Strasbourg, France, 11th edn, 2023.

41 L'équipe pédagogique de CheMoocs, August, 2023.

42 Y. B. Monakhova and D. N. Rutledge, *Talanta*, 2020, **208**, 120451.

43 A. Kassouf, D. Jouan-Rimbaud Bouveresse and D. N. Rutledge, *Talanta*, 2018, **179**, 538–545.